

XOR Gate Design Toward a Practical Complete Set for DNA Computing

著者	Nishijima Katsuhiro, Nakakuki Takashi
journal or publication title	New Generation Computing
volume	38
page range	285-301
year	2020-03-21
URL	http://hdl.handle.net/10228/00008088

doi: <https://doi.org/10.1007/s00354-020-00090-3>

XOR gate design toward a practical complete set for DNA computing

Katsuhiko Nishijima · Takashi Nakakuki

Received: date / Accepted: date

Abstract Practical design of the XOR gate is an important milestone in the field of DNA computing. In this study, we aim to develop an enzyme-free XOR gate driven by a toehold-mediated strand displacement mechanism possessing the true detection property. The advantages of our design are as follows: dual-rail logic is not required, the explicit use of the NOT gate is avoided, the circuit structure is simple, and the design is achievable with fewer DNA strands than that designed by the combination of four NAND gates. A rational circuit design is performed, and the dynamic behaviors of the biochemical reaction and the secondary structures of DNA strands are confirmed by computer simulation. In particular, both the domain-level design technique with G-T mismatched base pairs and base sequence-level fine-tuning are successfully achieved to alleviate the performance degradation arising from unintended and leaky reactions present in the circuit. The validity of the XOR gate design is confirmed by experimental studies.

Keywords Dynamic DNA nanotechnology · Strand displacement mechanism · Exclusive-OR gate

1 Introduction

Molecular programming using DNA strand displacement (DSD) has a long and rich history in the field of DNA dynamic nanotechnology [12]. Design

This work was supported by JSPS KAKENHI (grant no. 17K06500).

K. Nishijima
Department of Systems Design and Informatics, Kyushu Institute of Technology, Iizuka,
Fukuoka 8208502, Japan
Present address: Graduated in 2017.

T. Nakakuki
Department of Intelligent and Control Systems, Kyushu Institute of Technology, Iizuka,
Fukuoka 8208502, Japan E-mail: nakakuki@ces.kyutech.ac.jp

concepts enabling bottom-up, rational design of DNA molecular circuits have permitted the development of DNA circuits for various molecular machines, such as molecular robots [10]. Based on the beneficial characteristics of DSD, i.e., that we can consider a DSD reaction as an basic element with input and output channels in the circuit design, it has been proven that arbitrary systems of chemical equations are realizable *in vitro* by suitably connecting an output strand of a DSD reaction to an input strand of another DSD element to successfully create an ensemble of connected DSD elements (hereafter referred to as the DSD circuit) [18]. The study of DSD circuits has moved beyond proof-of-principle studies to relatively small circuits [1], and the major issue is the development of large-scale circuits comprised of a collection of some basic logical elements. To this end, the combinational circuit design must be established using a “complete set” for logic functions, where AND, OR, and NOT gates are a typical solution for the complete set in the sense that arbitrary Boolean functions are constructible in a combinational structure with these three gates [13]. In fact, this design principle provides a crucial cornerstone for electric circuit design.

Although AND, OR, and NOT gates have been already realized as a DSD circuit in many studies [17,14], it is unclear whether middle- or large-scale DSD circuits can be developed with this complete set for practical applications, and the circumstances are quite complex. As reported in previous studies [13, 14], the use of the NOT gate frequently causes problems because NOT gates generate a high concentration of output strand while consuming substrate or fuel strands, even before circuit operation. Thus, substrate and fuel strands required to drive the NOT gate are depleted. In addition to this dysfunction of the NOT gate, downstream gates could also react with the output of the NOT gate while consuming fuel strands before circuit operation. Because it would still be difficult to overcome the problems associated with the use of the NOT gate in a DNA combinational circuit, the main strategy for combinational circuit design is to utilize (i) dual-rail logic [9,17] or (ii) another complete set; indeed, in the field of Boolean algebra, various complete sets are known to exist [22].

For the former (i), Qian and colleagues proposed a complete set with only AND and OR gates by applying dual-rail logic, allowing them to avoid the explicit use of the NOT gate in the design of NAND, NOR, and XOR gates [13,14]. However, dual-rail logic requires two types of subsignals (x^0 and x^1) for defining a main signal (x) in a DNA circuit, where x^0 and x^1 correspond to the logical “low” and “high”, respectively. In this context, for example, the logical low of x is given by a combination of the high level of x^0 and low level of x^1 ; similarly, the logical high is given by a combination of the low level of x^0 and high level of x^1 . Although dual-rail logic is a powerful tool to construct large-scale DNA circuits [21], “true detection of the absence of input” (hereafter referred to as the true detection property), a major property of Boolean circuits, cannot be handled [6], where a logic circuit is said to have the property of “true detection of the absence of input” if the logical high and low of the input signal correspond to the high and low of the concentration of the

input molecule, respectively [4]. As for the latter (ii), Soloveichik and colleagues established a method for constructing arbitrary chemical reaction networks by introducing unimolecular ($X \rightarrow Y + Z$) and bimolecular ($X + Y \rightarrow Z$) reactions [18], where X , Y , and Z denote single-stranded DNA molecules, which corresponds to a complete set with “implication” [22]. This remarkable method encourages many researchers to develop “analog” DNA circuits with specific functions for various application purposes [11, 19, 16].

Other promising selections for complete sets without the NOT gate include those containing the XOR gate, such as {XOR, AND} and {XOR, OR}, because the XOR gate essentially contains the characteristics of the NOT gate; indeed, the XOR function can be theoretically assembled by the NOT function along with the OR or AND functions. However, the realization of an ideal XOR gate possessing the true detection property is still challenging in the field of DNA computing, although some studies have reported the XOR gates using dual-rail logic [15, 3] or enzymatic mechanisms [20, 8].

In this study, we develop an enzyme-free XOR gate possessing the true detection property for rational combinational circuit design by the complete set with the XOR gate. Our design has the following advantage: (i) dual-rail logic is not used, (ii) explicit use of the NOT gate is avoided, and (iii) because of the circuit size, the number of strands in the DNA circuit is considerably small. Inspired by the operation principle of the XOR gate based on pseudorotaxane formed by self-assembly of a wire-type electron acceptor and a macrocyclic electron donor [5], we establish different approaches to suppress the output status to logical low when the two input statuses are both logical high. Rational circuit design is performed, and the dynamic behaviors of the biochemical reaction and secondary structures of DNA strands are determined by computer simulation. Technically, both the domain-level design technique with G-T mismatched base pairs [7] and base sequence-level fine-tuning are successfully achieved to alleviate the performance degradation arising from unintended and leaky reactions present in the circuit. The validity of the XOR gate design is then confirmed by experimental studies.

2 New XOR gate design

2.1 Principle of circuit operation

An overview of our two-input XOR gate is depicted in Fig. 1A, where the inputs (I_1 and I_2) and output (O) strands are single-stranded DNA (ssDNA), and the predefined strands (G_1 , G_2 , F_1 , and F_2) are double-stranded DNA (dsDNA) with initial concentrations. The truth table of the XOR operation is given in Fig. 1B, where an input status of a high level of I_1 or I_2 leads to a high level of O ; otherwise, a low output is obtained.

Fig. 1C shows the detailed reaction processes in the circuit operation. In the case (1), i.e., the input status with a logical high I_1 and low I_2 (denoted as $(I_1, I_2) = (H, L)$), the input strand I_1 binds to the gate G_1 at the toehold do-

main and then released both the signal strand S_1 and the terminator strand T_1 via toehold-mediated strand displacement (TMSD), while generating a waste strand ($\mathbf{rxn} \alpha_1$ in Fig. 1C). Subsequently, S_1 in turn binds to the fuel strand F_1 , generating both the output strand O and a waste via TMSD ($\mathbf{rxn} \beta_1$); T_1 and F_2 form a waste complex ($\mathbf{rxn} \gamma_1$). Case (2) can be explained by the same mechanism as case (1), alternating the subscript numbers from “1” to “2”, and vice versa. In case (3), it is obvious that no output is generated because no reactions occur without no inputs. In case (4), the administration of both I_1 and I_2 leads to the generation of T_1 , S_1 , T_2 , and S_2 via TMSD ($\mathbf{rxns} \alpha_1$ and α_2). Because the fuel strand binds to the terminator strand much faster than the signal strand, no output is generated because the subsequent reaction after $\mathbf{rxns} \alpha_1$ and α_2 is dominated by fuel-terminator binding, resulting in the formation of a waste complex ($\mathbf{rxns} \gamma_1$ and γ_2). Taken together, the circuit operation determined by cases (1) to (4) coincides with the truth table shown

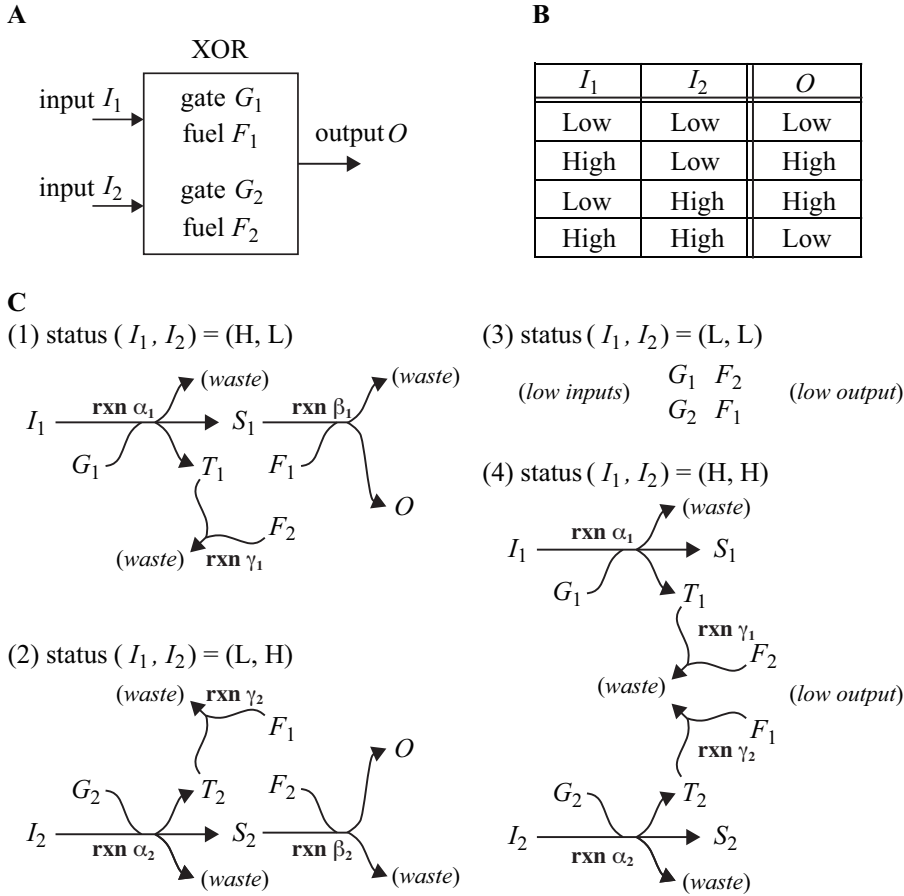


Fig. 1 Circuit operation of our XOR gate

in Fig. 1B, which indicates that the XOR gate is designed to have the true detection property.

In order to confirm the circuit operation principle, we perform numerical simulations based on chemical kinetics [24]. Our XOR gate can be mathematically described by the following ordinary differential equations:

$$\begin{aligned}
d[I_1]/dt &= -k_{f_a}[I_1][G_1], \\
d[G_1]/dt &= -k_{f_a}[I_1][G_1], \\
d[I_2]/dt &= -k_{f_a}[I_2][G_2], \\
d[G_2]/dt &= -k_{f_a}[I_2][G_2] \\
d[S_1]/dt &= k_{f_a}[I_1][G_1] - k_{f_b}[S_1][F_1], \\
d[T_1]/dt &= 2k_{f_a}[I_1][G_1] - k_{f_a}[T_1][F_2], \\
d[S_2]/dt &= k_{f_a}[I_2][G_2] - k_{f_b}[S_2][F_2], \\
d[T_2]/dt &= 2k_{f_a}[I_2][G_2] - k_{f_a}[T_2][F_1], \\
d[F_1]/dt &= -k_{f_b}[S_1][F_1] - k_{f_a}[T_2][F_1], \\
d[F_2]/dt &= -k_{f_b}[S_2][F_2] - k_{f_a}[T_1][F_2], \\
d[O]/dt &= k_{f_b}[S_1][F_1] + k_{f_b}[S_2][F_2],
\end{aligned} \tag{1}$$

where bracket $[\cdot]$ denotes the concentration of a strand, and the parameters k_{f_a} and k_{f_b} are association rate constants. We assume that the terminator strands are generated at more than twice the abundance of signal strands as described by the coefficient “2” in the right-hand sides of T_1 and T_2 ; this permits the terminator strands to suppress the output generation in case (4). Moreover, based on the specifications of our XOR gate with $k_{f_a} \gg k_{f_b}$, we set these values as $k_{f_a} = 3 \times 10^6$ ($\text{M}^{-1}\text{sec}^{-1}$) and $k_{f_b} = 5 \times 10^3$ ($\text{M}^{-1}\text{sec}^{-1}$) according to the feasibility of implementation of DNA base sequences (see Table 2 in Section 2.2.4 and Discussion section for details). The simulation results are shown in Fig. 2, where the initial concentrations are given in Table 1, and the output concentration is normalized according to the maximum value in time-course data for all four cases. Then, we confirm that our XOR gate has the true detection property and works successfully as expected in all four cases, indicating that the operation principle is theoretically adequate.

Table 1 Initial concentrations

strands	concentrations (nM)
I_1	0 or 100
I_2	0 or 100
G_1	100
G_2	100
F_1	100
F_2	100

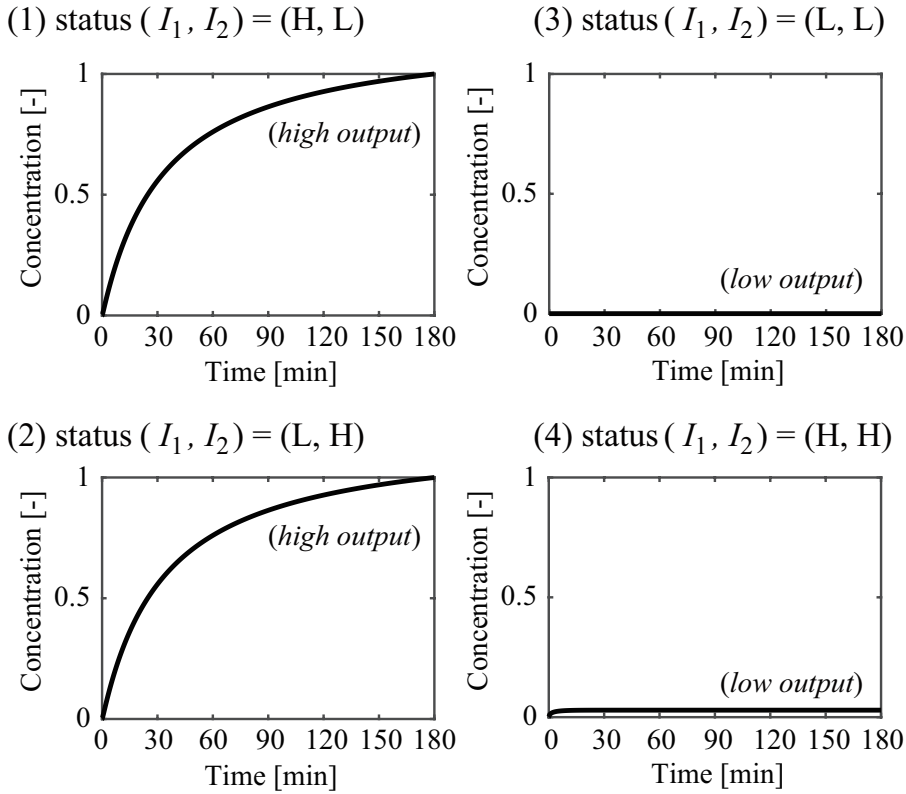


Fig. 2 Simulation results for our XOR gate

2.2 Implementation using DNA base sequences

The design procedure for the DNA circuit is summarized as follows. First, for each of the symbolic notations of DNA strands (I_1 , F_1 , etc.), its domain structure is designed such that the main reactions shown in Fig. 1 occur. Second, if harmful crosstalk that can ruin the normal circuit operation arises from complementary domains, the mismatch technique [2] is applied to the controversial domains to alleviate crosstalk binding. Finally, for each of the designed domains, the base sequence is designated while avoiding harmful secondary structures and inserting a short “clamp” domain to reduce leaky reactions [17].

2.2.1 Domain-level representation

The domain structure of each DNA strand in the XOR gate is designed as shown in Fig. 3, where the DNA strand is indicated by an arrow and the 3' end is indicated by an arrowhead. The region t_i ($i = 1, \dots, 6$) denotes a toehold domain that serves as a starting point for TMSD, s_i ($i = 1, \dots, 7$) denotes a

branch migration domain, and t_i^* ($i = 1, \dots, 6$) and s_i^* ($i = 1, \dots, 7$) denote the complementary domains of t_i and s_i , respectively. The binding domain forming the double helix structure is depicted by hatching. For better visibility in the figure, a small space is inserted between domains, which are connected with a thin line.

In accordance with the specifications of the XOR circuit, the terminator strands T_1 and T_2 need to have sufficient ability to suppress the output generation in case (4), as modeled by the coefficient 2 in the right-hand sides of the differential equation for T_1 and T_2 in Eq. (1). Hence, gates G_1 and G_2 are designed to contain double T_1 and T_2 strands in their structures, respectively. In addition to structural considerations, the differential equation (1) has two types of association rate constants with the relationship $k_{f_a} \gg k_{f_b}$, enabling more rapid binding of the terminator strand to the fuel strand than to the signal strand. Because the association rate constant of TMSD is tunable by changing the length of the relevant toehold domain [24], the toehold domains of the terminator strands T_1 and T_2 are given by $t_2 - t_3$ and $t_6 - t_4$ domains, respectively, and those of the signal strands S_1 and S_2 are given by t_4 and t_3 domains, respectively. This design rationally ensures the condition $k_{f_a} \gg k_{f_b}$, where k_{f_a} is determined by the length of the toehold $t_2 - t_3$ (or $t_6 - t_4$), and k_{f_b} is determined by the length of the toehold t_4 (or t_3) (also see Table 2 in Section 2.2.4 for a specific example).

2.2.2 Technical problems caused by crosstalk

Although the domain structures designed in Fig. 3 realize the intended reactions **rxns** $\alpha_1, \alpha_2, \beta_1, \beta_2, \gamma_1$, and γ_2 , two unintended reactions are also induced by domain complementarity, as shown in Fig. 4. The intended reaction is the main signal flow, whereas the unintended reaction is a ‘‘crosstalk’’ between signals. This could then ruin the normal operation of a circuit. Fig. 4A explains the crosstalk reaction between input I_1 and fuel F_2 , mediated by toehold $t_2 - t_3$ (**rxn** δ_1). In this case, this crosstalk is inevitable; in principle, I_1 and T_1 partially contain the same domain structures $t_2 - t_3 - s_2$ because **rxn** α_1 is a TMSD to exchange I_1 for T_1 . However, according to our specifications, T_1 is designed to bind to F_2 , which is why the crosstalk occurs and is unavoidable. Similarly, Fig. 4B illustrates a similar mechanism of crosstalk between input I_2 and fuel F_1 , mediated by the toehold $t_6 - t_4$ (**rxn** δ_2). In practical applications, the harmful effects of crosstalk on the main signal flow are circuit-dependent. Indeed, we experimentally confirmed that the XOR circuit could not operate correctly (data not shown). Therefore, some kind of measure is needed to reduce the effects of crosstalk.

2.2.3 Redesign using the mismatch technique

One effective measure is to suppress crosstalk reactions by breaking the complementarity of the toehold domain involved in the crosstalk reaction. The redesign strategy for the XOR gate can be outlined as follows. First, for **rxn**

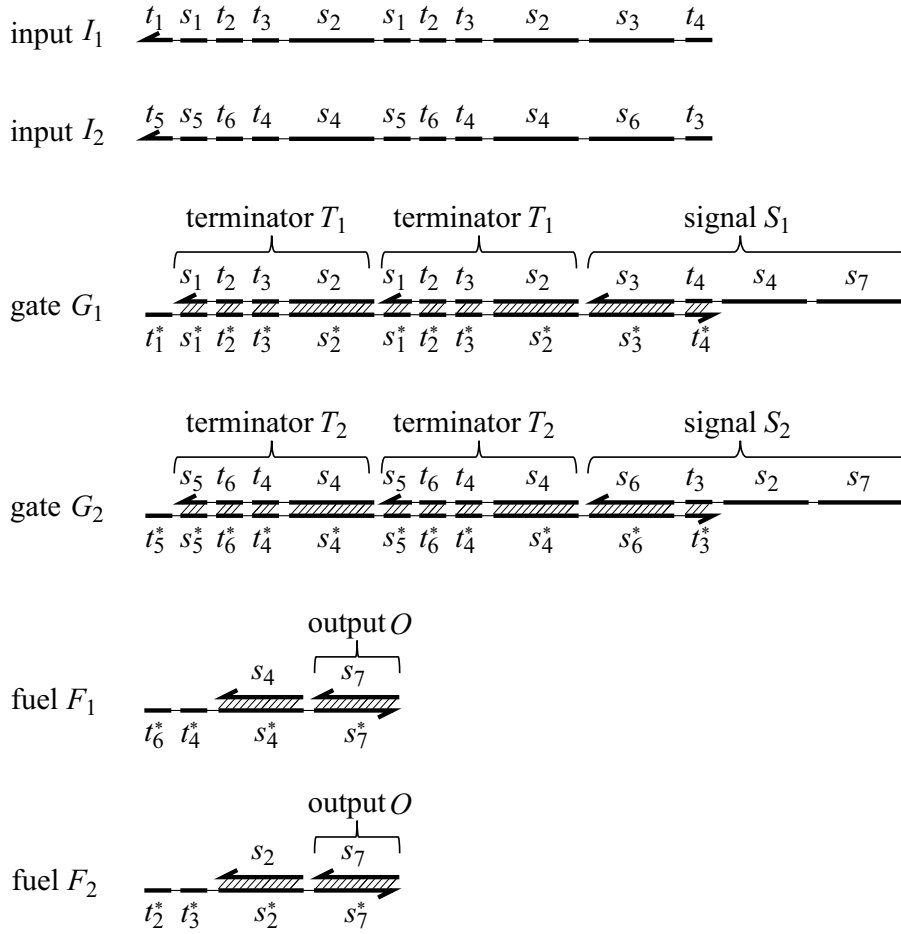


Fig. 3 Domain-level design of our XOR gate.

δ_1 , two toehold domains t_2^* and t_3^* of F_2 are replaced with \hat{t}_2^* and \hat{t}_3^* not to bind to their counterparts t_2 and t_3 of I_1 (Fig. 5A). However, these replacements destroy the intended reactions $\text{rxn } \gamma_1$ between F_2 and T_1 because the relevant toeholds involved in the TMSD become incompatible. Therefore, in turn, two toehold domains t_2 and t_3 of T_1 are replaced with \hat{t}_2 and \hat{t}_3 to bind to their counterparts \hat{t}_2^* and \hat{t}_3^* of F_2 for $\text{rxn } \gamma_1$ (Fig. 5A). Again, these replacements ruin the double helix structure of G_1 because of a lack of complementarity between the two domains $\hat{t}_2 - \hat{t}_3$ and $t_2^* - t_3^*$. In order to recover the double helix structure of G_1 , noncomplementary base pairs between $\hat{t}_2 - \hat{t}_3$ and $t_2^* - t_3^*$ are repaired using G-T mismatches, which exhibit the strongest binding affinity of all mismatched base pairs (Fig. 5B). It is reasonably expected that the double helix structure of G_1 can be formed by appropriately selecting the base sequences because this dsDNA is created by annealing (see Fig. 7 for

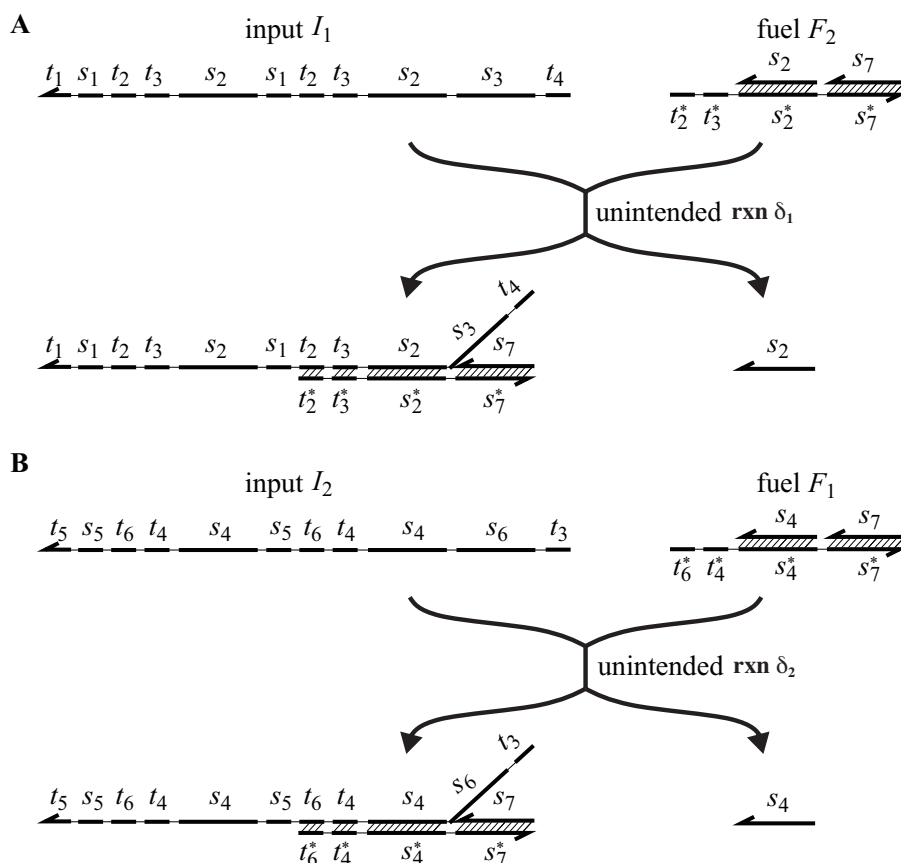


Fig. 4 Inevitable crosstalk reactions.

an example). Likewise, a similar redesign is applicable to F_1 , T_2 , and G_2 to suppress rxn δ_2 . As a result, by going through a series of modifications of the base sequences while making the use of G-T mismatching, it would be possible to suppress the unintended reactions rxns δ_1 and δ_2 while maintaining the intended reactions rxns α_1 , α_2 , β_1 , β_2 , γ_1 , and γ_2 .

Redesign by making use of G-T mismatch base pairs is generalized as follows. For simplicity, we consider a simple (toy) case. Suppose that we want to design a series of reactions such that strand 1 binds to strand 2, strand 2 binds to strand 3, strand 3 binds to strand 4, and but strand 4 does not bind to strand 1. However, if we design their base sequences just based on complementarity, it is unavoidable that strand 1 would bind to strand 4 (Fig. 5C). In contrast, if it is acceptable to use G-T mismatched base pairs between strands 2 and 3, strand 1 would not bind to strand 4 (Fig. 5D). Typically, such G-T mismatches are applicable when bonds of strands 2 and 3 are prepared by annealing.

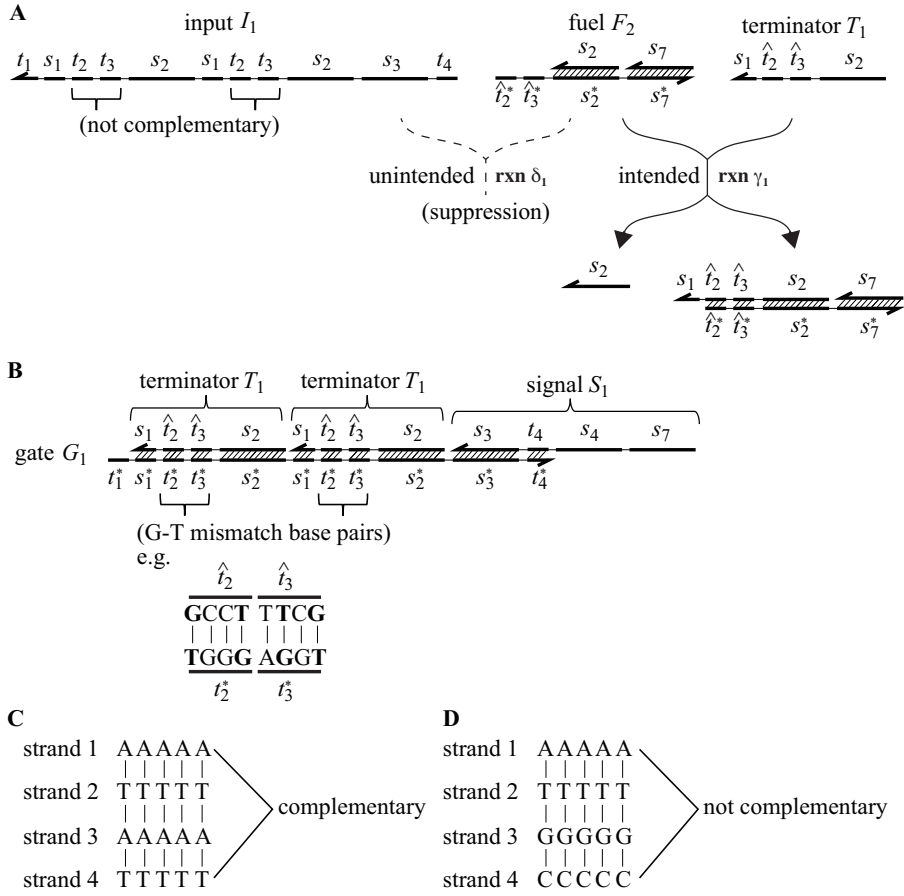


Fig. 5 Redesign by using G-T mismatched base pairs.

2.2.4 DNA base sequence design

DSD circuits frequently suffer from some types of leaky reactions that do not appear in the ideal reaction scheme expected by the domain structures of strands. In this case, a “fuel-gate leak” that contaminates the reaction scheme depicted in Fig. 1 may exist. Fig. 6A shows the leaky reaction ($\mathbf{rxn} \lambda_1$) between fuel F_1 and gate G_1 , where zero-toehold strand displacement may occur [13]. Such leaky reactions can be eliminated by inserting a clamp domain in the original domain structure [17]. Hence, the clamp domains s_{4a} and s_{4a}^* are inserted next to domains t_4 and t_4^* for G_1 , respectively, as shown in Fig. 6B; this could suppress $\mathbf{rxn} \lambda_1$. In response, input I_1 , which is a counterpart of G_1 , also needs to be added to the clamp domain s_{4a} , as depicted in Fig. 6C. Similar insertion of clamp domains is applicable to I_2 , G_2 , and F_2 .

Finally, Tables 2 and 3 summarize the length of each domain and the base sequence of each strand. Fig. 7 demonstrates the results of analysis of nucleic

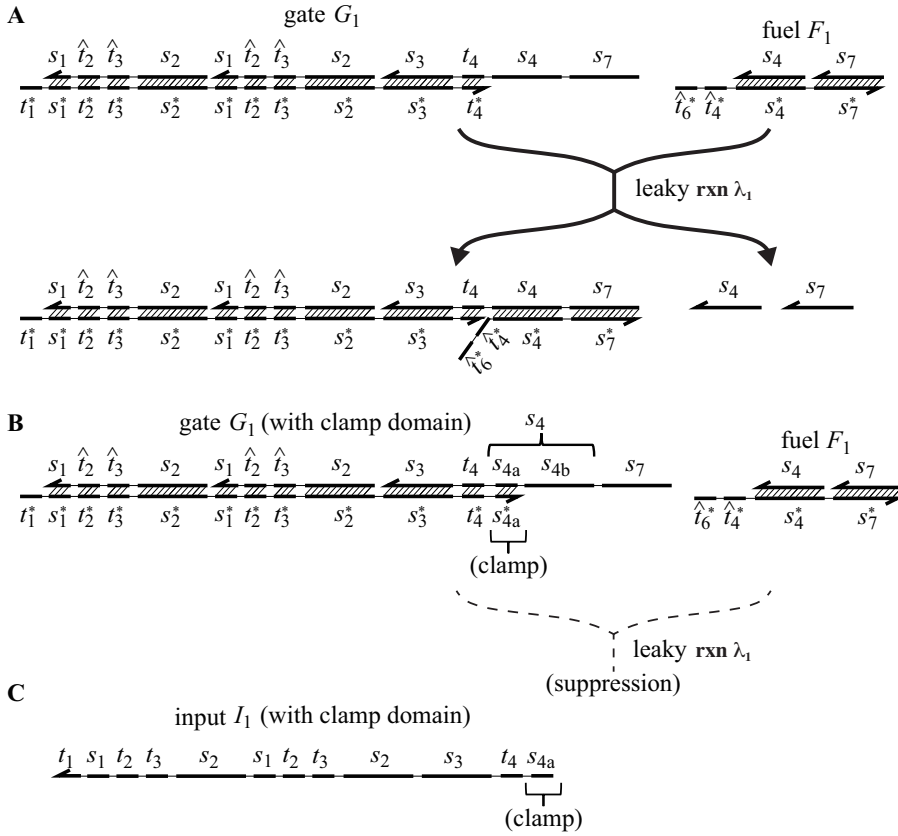


Fig. 6 Fuel-gate leak between G_1 and F_1 .

Table 2 Lengths of domains

domain	s_1	s_{2a}	s_{2b}	s_3	s_{4a}	s_{4b}	s_5	s_6	s_7
length [nt]	5	3	12	22	3	12	5	22	15

domain	t_1	t_2	t_3	t_4	t_5	t_6
length [nt]	7	4	4	4	7	4

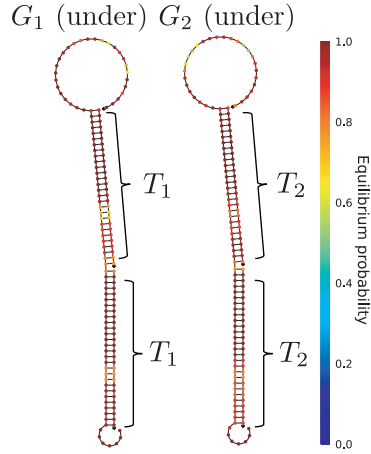
acid structures by NUPACK [23] to examine the validity of G-T mismatched base pairs between G_1 (under) and T_1 and between G_2 (under) and T_2 , respectively, indicating that double helix structures are successfully formed.

3 Experimental verification

Materials and methods are summarized in the Appendix. Fig. 8 shows the experimental results of time-course responses of output O under four types of input statuses, where the input concentrations of the logical low and high

Table 3 DNA base sequences

strands	base sequences (5' end → 3' end)
I_1	CCTACCATTACATTCATTTCCCTCCTTACCCTATCCAATTCGCCACCTCCCACA- -CACCCCTATCCAATTCGCCACCTCCCACACACTACCCTC
I_2	GCCACCTATAACCCACCATTTAACCCCTCCCTCCATATTCCTTACCAACCTTT- -TCCCTCCATATTCCTTACCAACCTTTTCCCTAACTT
G_1 (under)	GAGGGTAGTGTGTGGGAGGTGGCGAATTGGATAGGGTGTGTGGGAGGTGGC- -GAATTGGATAGGGTAAGGAGGGAATGAATGTAATGGTAGG
T_1	CCTATCCAATTCGCCGCTTTCCGCACAC
S_1	ACCCTTATCTCGCCCTCCATATTCCTATCGTTACATTCATTTCCCTCCTTAC
G_2 (under)	AAGTTAGGGAAAAGGTTGGTAGGAGAATATGGAGGGGAAAAGGTTGGTAGGA- -GAATATGGAGGGAAGGGTTAAATGGTGGGTTATAGGTGGC
T_2	CCTCCATATTCCTATCGGCTTTTTTCC
S_2	ACCCTTATCTCGCCCTATCCAATTCGCCGCTTATAACCCACCATTTAACCCCTTC
F_1 (under)	AAGCCGATAGGAGAATATGGAGGGCGAGATAAGGGTGG-[BHQ]
F_1 (upper)	CCTCCATATTCCT
F_2 (under)	CGGAAAGCGGCGAATTGGATAGGGCGAGATAAGGGTGG-[BHQ]
F_2 (upper)	CCTATCCAATTCGCC
O on F_1	[Cy5]-CCACCCTTATCTCGC
O on F_2	[FAM]-CCACCCTTATCTCGC

**Fig. 7** Analysis of nucleic acid structures (NUPACK[23]).

are 0 and 100 nM, respectively. Other initial concentrations are summarized in Table 1. Because output O is mounted on both F_1 and F_2 , as shown in Figs. 3, Cy5 and FAM fluorophores are labeled for output strands mounted on F_1 and F_2 , respectively, to distinguish which fuel strand is the source of the output (see Table. 3). In addition, simulation results are included as a comparison. To make the comparison easier in terms of the transient property, the simulation curve is normalized to match at the final time point (135 min) of the experimental data in Figs. 8B and C.

For the input status $(I_1, I_2) = (L, L)$, both Cy5- and FAM-labeled outputs remained low, although the data tended to increase slightly over time owing to leaky reactions. For the input status $(I_1, I_2) = (H, L)$, only Cy5-labeled

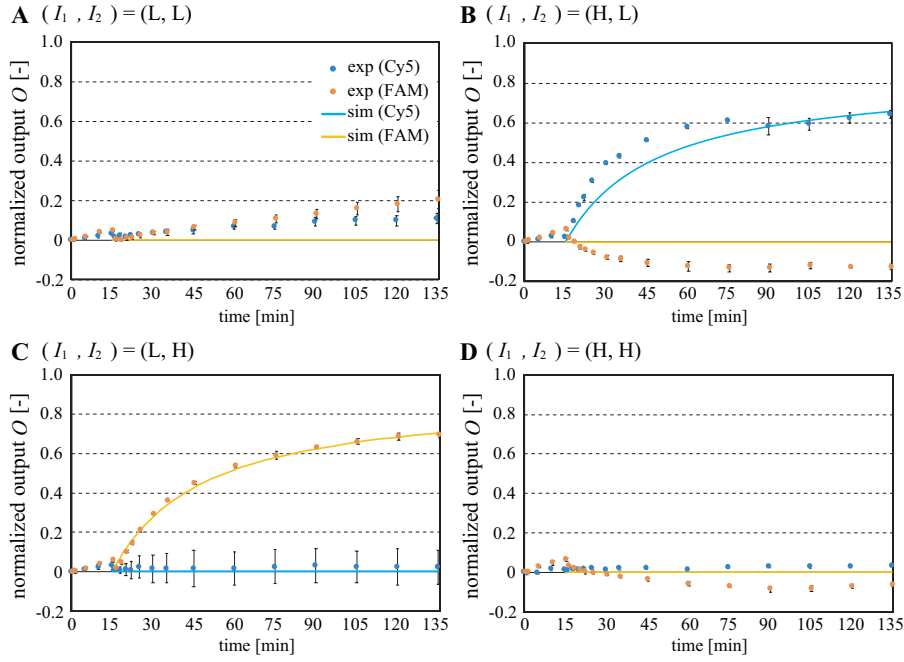


Fig. 8 Experimental results of our XOR gate.

output increased to a high level, whereas FAM-labeled output did not appear. Inversely, for the input status $(I_1, I_2) = (L, H)$, only FAM-labeled output increased to a high level, whereas Cy5-labeled output did not appear. For the input status $(I_1, I_2) = (H, H)$, no output responses are observed, indicating that terminator strands suppressed the generation of output by the fuel strand by binding to the fuel strand much faster than binding between fuel and signal strands, as shown in Fig. 1. Taken together, our experimental results confirmed that the designed circuit successfully functioned in accordance with the truth table for the XOR operation with the true detection property.

4 Discussion: reaction rate constants

The reaction rate constants of TMSD can be “estimated” reasonably based on the lengths of toehold sequences in accordance with the calculus given in a previous study [24]. In our simulation, we assume that the lengths of toehold sequences related to the reaction rate constants k_{f_a} and k_{f_b} are the same between I_1 - and I_2 -induced reaction pathways. Therefore, we believe that our parameter setting would be reasonable from the perspective of simulation techniques in the field of DNA computing. On the other hand, the “actual” reaction rate constant is also affected by the type and combination of base sequences, particularly for GC content. For k_{f_a} , the association rate constant

of TMSD saturates if the corresponding toehold length is greater than six [24]. In our design shown in Table 2, the toehold lengths related to k_{f_a} are seven (t_1 for the $I_1 - G_1$ association, and t_5 for the $I_2 - G_2$ association) and eight ($t_2 - t_3$ for the $T_1 - F_2$ association, and $t_6 - t_4$ for the $T_2 - F_1$ association); therefore, k_{f_a} is saturated beyond the influence of differences in base sequences among toehold domains. For k_{f_b} , the GC contents of toehold sequences related to k_{f_b} are the same (e.g., “ATCG” for t_4 and “GCTT” for t_3); therefore, k_{f_b} may be a reasonable parameter in our validation simulation. In addition, the experimental results shown in Fig. 8 also demonstrate the validity of our design, even in cases of (high, high).

5 Conclusion

In this study, we developed an enzyme-free XOR gate made from a combination of TMSD reactions possessing the true detection property. Our XOR gate does not require dual-rail logic and can be realized with fewer types of DNA strands than that designed by a combination of four NAND gates. Circuit design is carried out based on a series of reasonable procedures, and the dynamic behaviors of the biochemical reaction and the secondary structures of DNA strands are confirmed by computer simulation. In DNA circuit design, unintended and leaky reactions significantly affect the success or failure of the design at the experimental level. Domain-level redesign using G-T mismatched base pairs is performed to mitigate unintended reactions, and sequence-level fine-tuning is achieved, along with using the clamp domain, to mitigate leaky reactions. Overall, our experimental results showed that the circuit design is effective.

A Materials and Methods

System Specifications. All DNA oligos in Table 3 are synthesized and purified by Nippon Gene, Co., Ltd (Tokyo, Japan). Each DNA oligo is diluted with $1\times$ TE buffer (Nippon Gene, Co., Ltd.) with 12.5 mM $MgCl_2$ added at concentrations shown in Table 1. The dsDNAs G_1 , G_2 , F_1 , and F_2 are prepared by annealing from 90 °C to 20 °C with a temperature gradient of -1 °C per min after heating at 90 ° for 15 min with a thermal cycler (GeneAtlas ASTEC325 by Astec Co., Ltd; Fukuoka, Japan).

Signal intensity measurements. After annealing, all samples are held for 30 min and are then mixed in test tubes, except for samples with input strands. Signal intensity measurements are performed with a fluorescence spectrophotometer (FP-8300; JASCO Co., Ltd.; Tokyo Japan) at a temperature of 20 °C, where the 5' end of the output O mound on F_1 is labeled with Cy5, the 5' end of the output O mound on F_2 is labeled with FAM, and the 3' ends of fuels F_1 and F_2 are labeled with the black fluorescence quencher BHQ (see Table 3). Input strands required for each experimental condition are added 15 min after the start of measurement, and observation of signal intensity is performed for 120 min. For FAM measurement, the excitation wavelength is 496 nm, and the fluorescence wavelength is 524 nm; for Cy5 measurement, the excitation wavelength is 643 nm, and the fluorescence wavelength is 667 nm.

Normalization of measured time-course data. For each experimental condition, three independent time series measurements are taken to determine the mean and standard

deviation. The fluorescence intensity before input administration is set to the minimum value. In the case of status $(I_1, I_2) = (L, L)$, after 2 h of measurement, excess amounts of I_1 and I_2 are added, and the average of the last five time-course points at which the fluorescence intensity converged is taken as the maximum value [13]. Using these minimum and maximum values, the experimental data are normalized to be in the range of 0 to 1.

References

1. Berleant, J., Berlind, C., Badelt, S., Dannenberg, F., Schaeffer, J., Winfree, E.: Automated sequence-level analysis of kinetics and thermodynamics for domain-level dna strand-displacement systems. *J. R. Soc. Interface* **15**(20180107) (2018)
2. Broadwater, D.W.B.J., Kim, H.D.: The effect of basepair mismatch on dna strand displacement. *Biophys J* **110**(7), 1476–1484 (2016)
3. Cardelli, L., Kwiatkowska, M., Whitby, M.: Chemical reaction network designs for asynchronous logic circuits. *Nat Comput* **17**(1), 109–130 (2018)
4. Chiniforooshan, E., Doty, D., Kari, L., Seki, S.: Scalable, time-responsive, digital, energy-efficient molecular circuits using dna strand displacement. *arXiv:1003.3275 [cs.OH]* (2010)
5. Credi, A., Balzani, V., Langford, S.J., Stoddart, J.F.: Logic operations at the molecular level. an xor gate based on a molecular machine. *J. Am. Chem. Soc.* **119**(11), 2679–2681 (1997)
6. Garg, S., Shah, S., Bui, H., Song, T., Mokhtar, R., Reif, J.: Renewable time-responsive dna circuits. *Small* **14**(1801470), 1–9 (2018)
7. Jian, Y.S., Bhadra, S., Li, B., Ellington, A.D.: Mismatches improve the performance of strand-displacement nucleic acid circuits. *Angew Chem Int Ed Engl* **53**(7), 1845–1848 (2014)
8. Lederman, H., Macdonald, J., Stefanovic, D., Stojanovic, M.N.: Deoxyribozyme-based three-input logic gates and construction of a molecular full adder. *Biochemistry* **45**(4), 1194–1199 (2006)
9. Muller, D.E.: Asynchronous logics and application to information processing. *Proc. Symp. Switching Theory in Space Technology* pp. 289–297 (1963)
10. Murata, S., Konagaya, A., Kobayashi, S., Saito, H., Hagiya, M.: Molecular robotics: A new paradigm for artifacts. *New Generation Computing* **31**(1), 27–45 (2013)
11. Oishi, K., Klavins, E.: Biomolecular implementation of linear i/o systems. *IET Syst. Biol* **5**(4), 252–260 (2011)
12. Padirac, A., Fujii, T., Rondelez, Y.: Nucleic acids for the rational design of reaction circuits. *Current Opinion in Biotechnology* **24**, 575–580 (2013)
13. Qian, L., Winfree, E.: Scaling up digital circuit computation with dna strand displacement cascades. *Science* **332**(6034), 1196–1201 (2011)
14. Qian, L., Winfree, E.: A simple dna gate motif for synthesizing large-scale circuits. *J. R. Soc. Interface* **8**(62), 1281–1297 (2011)
15. Qian, L., Winfree, E., Bruck, J.: Neural network computation with dna strand displacement cascades. *Nature* **475**, 368–372 (2011)
16. Sawlekar, R., Montefusco, F., Kulkarni, V.V., Bates, D.G.: Implementing nonlinear feedback controllers using dna strand displacement reactions. *IEEE Trans. NanoBiol.* **15**(5), 443–454 (2016)
17. Seelig, G., Soloveichik, D., Zhang, D.Y., Winfree, E.: Enzyme-free nucleic acid logic circuits. *Science* **314**(5805), 1585–1588 (2006)
18. Soloveichik, D., Seelig, G., Winfree, E.: Dna as a universal substrate for chemical kinetics. *PNAS* **107**(12), 5393–5398 (2010)
19. Song, T., Garg, S., Mokhtar, R., Bui, H., Reif, J.: Analog computation by dna strand displacement circuits. *ACS Synt Biol* **5**, 898–912 (2016)
20. Stojanovic, M.N., Mitchell, T.E., Stefanovic, D.: Deoxyribozyme-based logic gates. *J Am Chem Soc* **124**(14), 3555–3561 (2002)
21. Thubagere, A.J., Thachuk, C., Berleant, J., Johnson, R.F., Ardelean, D.A., Cherry, K.M., Qian, L.: Compiler-aided systematic construction of large-scale dna strand displacement circuits using unpurified components. *Nat. Comm.* **8**(14373), 1–12 (2017)

-
22. Wernick, W.: Complete sets of logical functions. *Transactions of the American Mathematical Society* **51**, 117–132 (1942)
 23. Zadeh, J.N., Steenberg, C.D., Bois, J.S., Wolfe, B.R., Pierce, M.B., Khan, A.R., Dirks, R.M., Pierce, N.A.: Nupack: Analysis and design of nucleic acid systems. *Journal of Computational Chemistry* **32**, 170–173 (2010)
 24. Zhang, D.Y., Winfree, E.: Control of dna strand displacement kinetics using toehold exchange. *J. AM. CHEM. SOC.* **131**, 17303–17314 (2009)